EVALUATION OF THE GEOMETRY OF SINGLE-LAP ADHESIVE JOINTS IN COMPOSITE LAMINATES

Elena M. Moya-Sanz*, Lorena M. Fernández-Cañadas*, Inés Iváñez* and Shirley K. Garcia-Castillo*

*Department of Continuum Mechanics and Structural Analysis
University Carlos III of Madrid
Avda. de la Universidad 30, 28911 Leganés, Madrid, Spain

e-mail: idel@ing.uc3m.es, web page: http://www.uc3m.es/mma

Keywords: composite, adhesive joints, cohesive zone model.

Abstract

In this work, the influence of geometry on the mechanical behaviour of single-lap adhesive joints has been analysed in order to evaluate its mechanical behaviour. Four configurations have been studied and compared: 1) single-lap joint, 2) adherends chamfering, 3) adhesive chamfering, and 4) adhesive and adherends chamfering. A 2D finite-element model has been developed using Abaqus/Standard, in which the adhesive behaviour has been defined by a Cohesive Zone Model (CZM). The analysis has been carried out in terms of failure load, peak peel stress, and peel stress distribution.

1. INTRODUCTION

The current significance of reducing environmental impact and the need of saving costs are fundamental issues in aircraft industry. The way to achieve those objectives is to reduce the structural weight in order to decrease the fuel consumption and increase the payload efficiency, as it is estimated that a reduction of 1 kg in structural weight of an Airbus A320, decreases in 2900 litres the fuel used per year [1]. In order to obtain this reduction, two strategies are followed: 1) Using lightweight materials as composites laminates to manufacture airframe structures, and 2) Using adhesive joints instead of mechanical joints.

Adhesive joints when compared to mechanical joints do not add structural weight and stress concentrators are removed because of absence of holes [2]. However, the load transfer and stress concentration in both adherents and adhesive are important parameters that must be studied.

Single-lap adhesive joints are the most used due to their simply geometry and efficiency of work. The main disadvantage of this type of joints is the eccentricity of the load, that causes bending in the adherents and great peel stresses in the extreme of the adhesive [3]. Of particular interest has been the analysis of different geometric configurations of single-lap joints with the aim of reducing the intensity of the stress peaks and therefore increase the strength of the joint.

In this work, different geometrical configurations of single-lap joint have been studied, such as adherent and adhesive chamfering. The main objective is to analyse the effect of these geometrical variations in the mechanical strength of the joint in terms of peel stress and failure load.

2. NUMERICAL STUDY

To study the influence of several geometrical variations on the strength of an adhesive single-lap joint, a 2D numerical model using the commercial finite-element code Abaqus/Standard was developed. The single-lap reference geometry was taken from the literature [4].

To reproduce the experimental conditions, one of the edges was fully clamped, while the opposite end was subjected to normal traction load by imposing a constant and uniform displacement through the opposite end (Fig. 1).

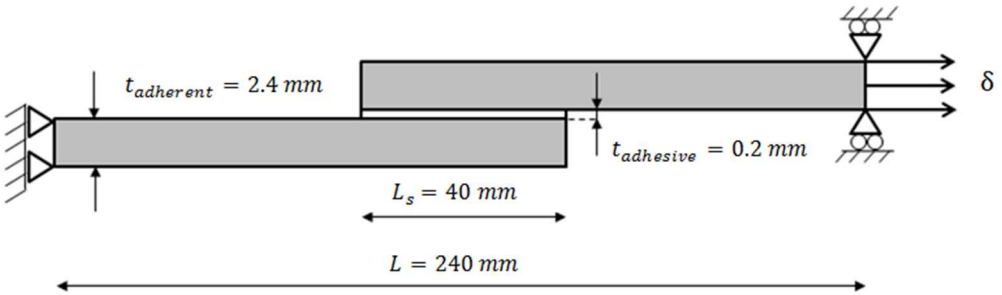

Figure 1. Problem description

The adherends were made of unidirectional carbon-epoxy pre-preg $[0]_{16}$ lay-up, with a thickness of 0.15 mm each ply, which properties are shown in Table 1.

Table 1. Elastic orthotropic properties of the adherends [4].

Elastic Modulus	$\mathbf{E_x}$ = 109 GPa
Elastic Modulus	$\mathbf{E_y}$ = 8.8 GPa
Shear Modulus	$\mathbf{G_{xy}}$ = 4.3 GPa
Poisson's ratio	$\mathbf{\nu_{xy}}$ = 0.342

The behaviour of the adhesive, Araldite 2015, was defined using Cohesive Zone Model (CZM) implemented in Abaqus/Standard, which reproduces the adhesive behaviour in terms of cohesive traction-separation response.

The initial behaviour is defined by a constitutive elastic matrix that relates the nominal stresses to the nominal strains across the interface (Eq. 1).

$$\begin{Bmatrix} t_n^0 \\ t_s^0 \end{Bmatrix} = \begin{bmatrix} K_{nn} & K_{ns} \\ K_{ns} & K_{ss} \end{bmatrix} \cdot \begin{Bmatrix} \varepsilon_n^f \\ \varepsilon_s^f \end{Bmatrix} \quad (1)$$

where t_n, t_s are the traction stresses in the normal and shear directions respectively, while ε_n, ε_s represent the strains in those same directions. K, is the stiffness matrix related to the adhesive properties (Table 2).

Table 2. Cohesive properties of Araldite 2015 [4].

E (GPa)	1.85	**t_n (MPa)**	21.6	**Gn (N/m)**	430
G (GPa)	0.56	**t_s (MPa)**	17.9	**Gs (N/m)**	4700

The onset of the degradation is given by a damage initiation criterion. In this work, a quadratic nominal stress criterion, available in Abaqus/Standard, has been chosen (Eq. 2):

$$\left\{\frac{\langle t_n \rangle}{t_n^0}\right\}^2 + \left\{\frac{t_s}{t_s^0}\right\}^2 = 1 \tag{2}$$

The material damage occurs according to a damage evolution law (Eq. 3), which describes the adhesive stiffness degradation rate:

$$d_{n,s} = \frac{\delta_{n,s}^f \cdot (\delta_{n,s} - \delta_{n,s}^0)}{\delta_{n,s} \cdot (\delta_{n,s}^f - \delta_{n,s}^0)} \tag{3}$$

In Eq. 3, a scalar damage variable, *d,* is defined to represent the overall damage in the adhesive. Initially, the behaviour of the adhesive is controlled by the elastic region, thus *d=0*. When the adhesive is fully damaged *d=1*. In this regard, different shapes of damage evolution, between the onset and complete failure, can be used. In this work, a linear damage evolution law has been chosen (Fig. 2).

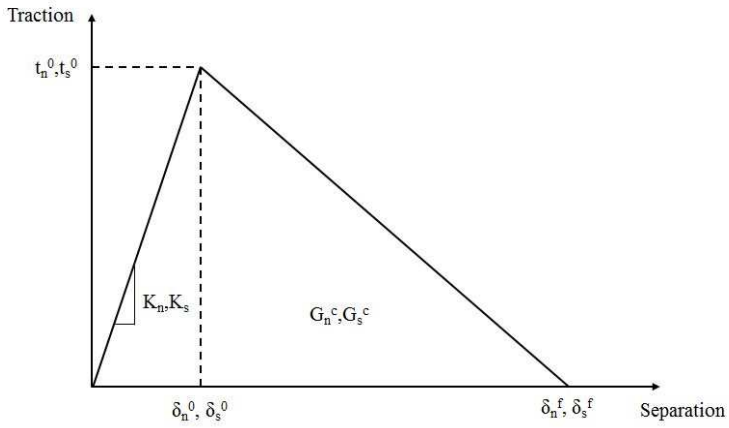

Figure 2. Damage evolution law considered (linear).

The sensitivity of the mesh was analysed in order to find an equilibrium solution between computational cost and accurate predictions of failure load. In this context, four-node linear plane strain elements (CPE4 in Abaqus) were used to mesh the adherends, while four-node linear cohesive elements (COH2D4 in Abaqus), were used to mesh the adhesive layer.

Four different joint configurations were studied. First configuration, configuration (1), corresponds to a single-lap joint with overlap lengths ranging from 10 mm to 80 mm (Fig. 3a). This is considered the reference case. Configuration (2) and configuration (3) consider adherends and adhesive chamfering, respectively (Fig. 3b and 3c), with chamfer angles between 15º and 90º. The last configuration, configuration (4), considers the chamber of adherends and adhesive simultaneously (Fig. 3d).

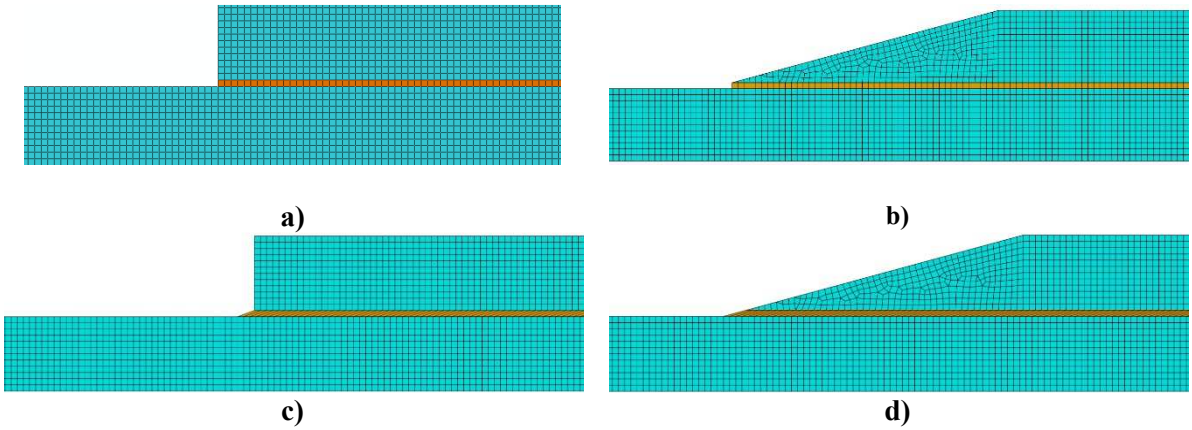

Figure 3. Detail of the numerical model mesh in different configurations: a) Single-lap joint, b) Adherents chamfering, c) Adhesive chamfering, d) Adherends and adhesive chamfering.

The numerical model results obtained were validated comparing with the experimental data available in the literature [4]. The variable used in the validation was the failure load as a function of the overlap length (Fig. 4).

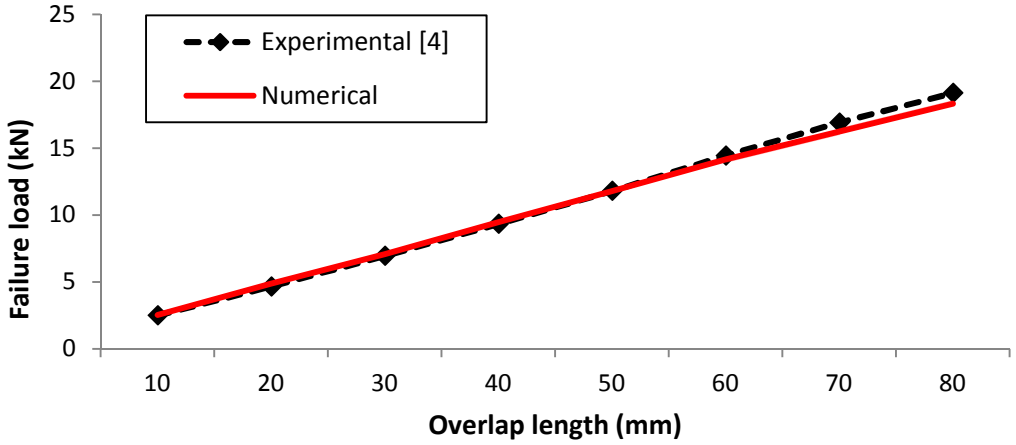

Figure 4. Comparison between experimental and numerical results: failure load vs. overlap length.

The numerical results are in good agreement with experimental data, as the differences between both results are less than 5%. Thus, the numerical model is validated.

3. RESULTS AND DISCUSSION

The strength of single-lap adhesive joints is analysed in terms of peak peel stress, peel stress distribution along the overlap length, and failure load of the joint. Values of the peak peel stress in the adhesive and failure load for the reference single-lap joint (presented in Fig. 1) are shown in Table 3.

Table 3. Results for single-lap joint in configuration (1).

Failure load	P_0 (kN)	9.46
Peek peel stress	σ_0 (MPa)	18.10

Fig. 5 shows the peel stress profile along overlap in the adhesive, caused by the eccentricity of the load, for configuration (1). The stress distribution is symmetrical and the maximum peel stresses appear at the ends of the adhesive, followed by a large gradient and a compressive region.

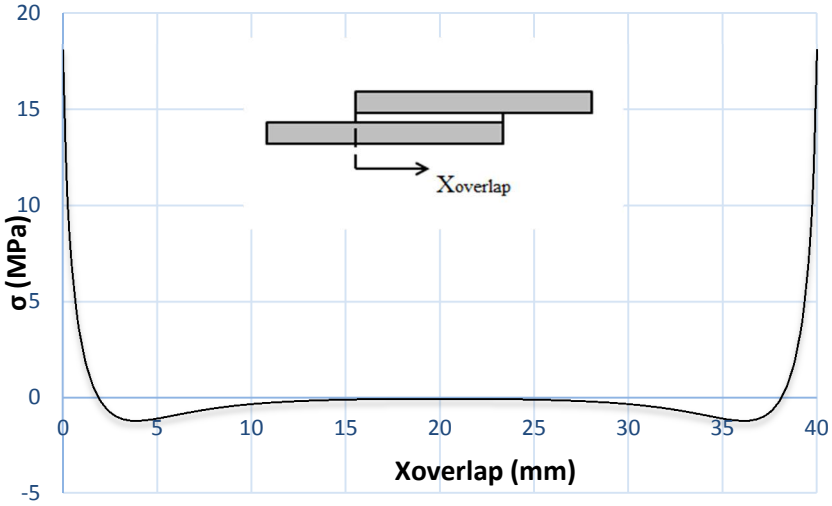

Figure 5. Peel stress profile of the adhesive in a single-lap joint.

In orden to evaluate the effect of some geometrical variations, results of configurations (2), (3) and, (4) are compared with configuration (1). Seven chamfer angles were analysed, between 90^0 to 15^0.

The variation of peak peel stress as a function of the chamfer angle is presented in Fig. 6. Results for configuration (1) are presented with a black broken line. Great reduction in peak peel stress is given in the case of adherends and adhesive chamfering, and the variation increases when the chamfer angle decreases its value.

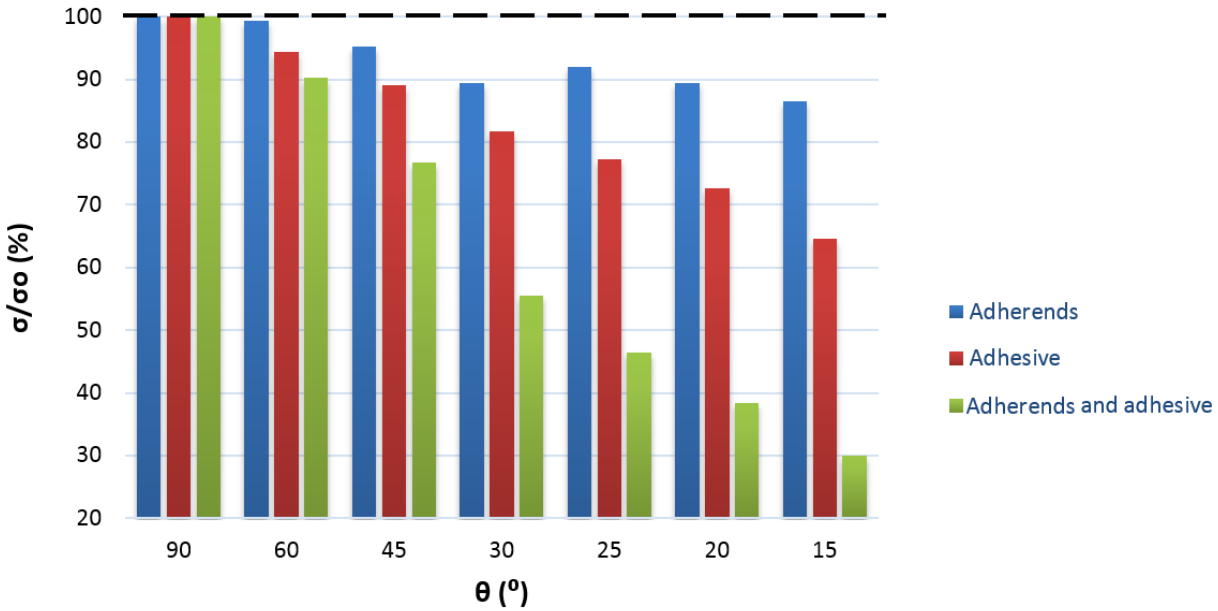

Figure 6. Peak peel stress of adhesive results for chamfering

The value of the peak peel stress decrease around a 70% with respect to the reference configuration for chamfer angle of 15°. The reduction of the peak peel stress can be explained as follows: the change of the cross-section at the end of the overlap is more gradual in joints with chamfers than in the reference configuration, thus the stress concentration factor in that point decreases.

Fig. 7 shows the peel stress distribution along the adhesive overlap for the reference single–lap joint, configuration (1), and adherents and adhesive chamfering, configuration (4), with a chamfer angle of 15^0.

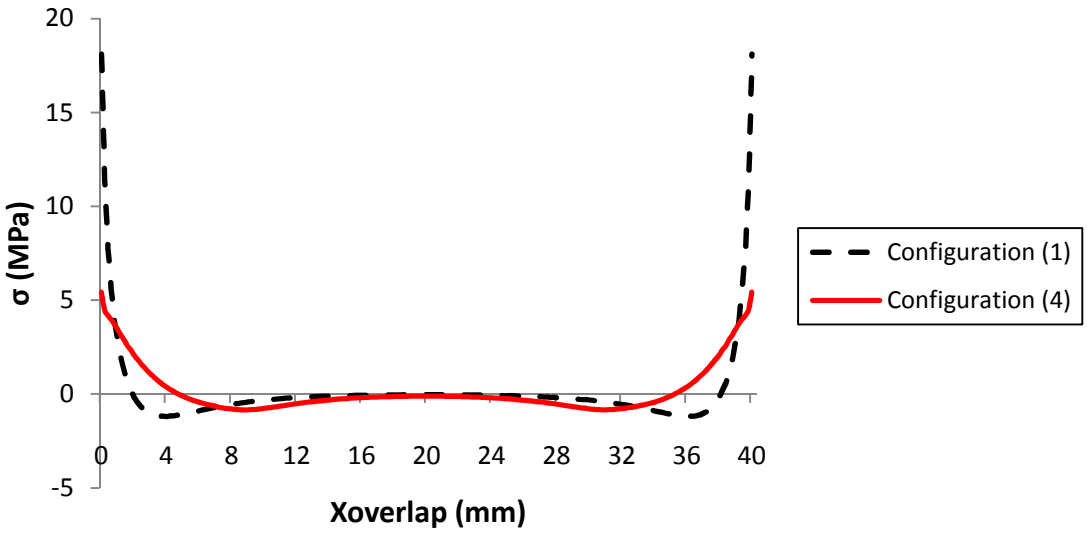

Figure 7. Peel stress distribution for configurations (1) and (4), at chamfer angle of 15º

In all cases studied, the peel stress distribution is symmetric: it shows a peak peel stress at the free ends of the adhesive, followed by a zone of compression. A great reduction of the peak peel stress can be observed for adherents and adhesive chamfering.

In general, the peak peel stress is much higher than the one given in the rest of the overlap. This means that the value of the stress distribution along the overlap is negligible with respect to the value of the peak peel stress at the end of the overlap.

Fig. 8 shows the failure load for different configurations as a function of the chamfer angle. An increment in the failure load occurs in all configurations studied with respect to the reference case. A clear trend can be observed: failure load increases when chamfer angle decreases.

It is observed that the increment of failure load is more noticeable in results of adherends chamfering than in adhesive chamfering. The failure load increases significantly for angles smaller than 45º. The highest failure load is achieved at chamfer angle of 15^0 and for adherends and adhesive chamfering.

These results show that modifications on the joint end geometry, as chamfering, spread the load transfer over a larger area and gives a more uniform shear stress distribution, increasing the performance of the joint.

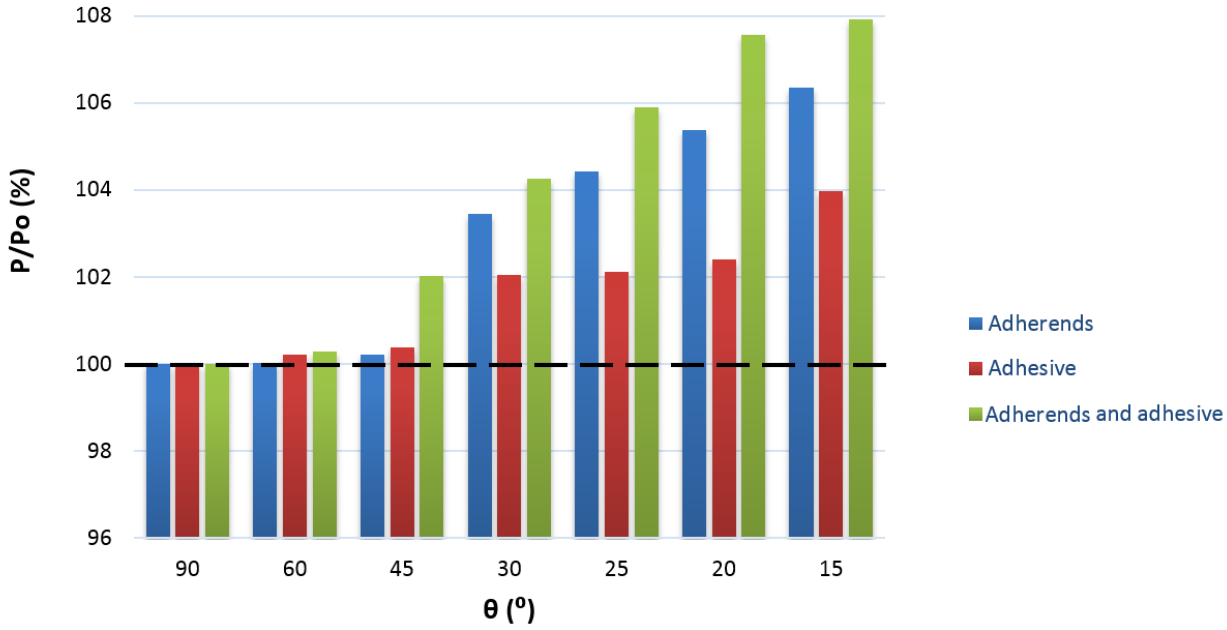

Figure 8. Failure load results for chamfering

The configuration with less peak peel stress is coincident with the one with the highest failure load: chamfering both adherends and adhesive at 15^0.

4. CONCLUSIONS

The aim of this work is to analyse the effect of geometrical variations in the performance of the mechanical strength of a single-lap joint. A 2D finite-element model has been developed using Abaqus/Standard. The joint is subjected to uniaxial tensile load, considering only cohesive failure. The analysis have been carried out in terms of failure load, peak peel stress, and peel stress distribution along the overlap.

It was found that the best configuration of all studied geometrical variations is chamfering adherends and adhesive, at the same time, with chamfer angle of 15°. When the chamfer angle decrease, the peak peel stress is reduced and the failure load increases.

The reduction of peak peel stress in the case of adherends and adhesive chamfering is a consequence of a reduction in the eccentricity of the load and the gradual change of cross-section at the end of the overlap, which avoid the stress concentration at that point. Also, the strength of the joint increases because of a better load transfer through the adhesive in the case on chamfering with respect to the reference configuration.

Acknowledgments

The authors are indebted for the financial support of this work to the Ministry of Economy and Competitiveness of Spain (project DPI2013-42240-R).

References

[1] R.M. O'Higgins, M.A. McCarthy, C.T. McCarthy. Comparison of open hole tension characteristics of high strength glass and carbon-fibre-reinforced composite materials. *Composite Science and Techonology*. 68: 2770-2778 (2008).

[2] K. Kwang-soo, Y. Yeong-Moo, C. Gwan-Rae, K. Chun-Gon. Failure prediction and strength improvement of uni-directional composite single lap bonded joints. *Composites Structures*. 72:477-485 (2006).

[3] M.D. Banea, L.F.M. Da Silva. Adhesively bonded joints in composite materials: an overview, *Proceedings of the institution of Mechanical Engineers, Part L: J of Materials Design and Applications.* 223 (2009).

[4] R.D.S.G.Campilho, M.D.Banea, J.A.B.P.Neto, L.F.M.da Silva. Modelling adhesive joints with cohesive zone models: effect of the cohesive law shape of the adhesive layer. *International Journal of Adhesive and Adhesion*. 44:48-56 (2013).